SEMARAK ILMU PUBLISHING

Journal of Advanced Research in Fluid Mechanics and Thermal Sciences

Journal homepage:
https://semarakilmu.com.my/journals/index.php/fluid_mechanics_thermal_sciences/index
ISSN: 2289-7879


# Air Flow Analysis and Effect of Angle on Rotation Vane Blade Through 90-Degree by Computational Fluid Dynamic

Wan Alif Mustaqim Wan Hashim[1], Nurul Farhanah Azman[1], Mohamad Nor Musa[1,*], Syahrullail Samion[1,2], Nor Azwadi Che Sidik[3], Yutaka Asako[3]

[1] School of Mechanical Engineering, Universiti Teknologi Malaysia, 81310 UTM Skudai, Johor, Malaysia
[2] Institute for Vehicle Systems and Engineering (IVeSE), Universiti Teknologi Malaysia, 81310 UTM Skudai, Johor, Malaysia
[3] Malaysia-Japan International Institute of Technology (MJIIT), Universiti Teknologi Malaysia, Jalan Sultan Yahya Petra, 54100 Kuala Lumpur, Malaysia

**ARTICLE INFO**

***Article history:***
Received 3 February 2022
Received in revised form 25 April 2022
Accepted 27 April 2022
Available online 26 May 2022

***Keywords:***
90° pipe bend; vane blade; numerical study; pressure drop

**ABSTRACT**

The effects of different angles of rotation vane blades on the flow characteristics in a pipe bend were numerically examined in this work using computational fluid analysis (CFD). The model's geometry included a straight inlet pipe of 1 m length, a 90° pipe bend with a 0.1 m cross-section diameter, a straight outlet pipe of 1 m length, and the installation of rotating vane blades at 10° and 33° angles. The simulation's input parameters include fluid viscosity (0.000017894 kg/m.s), fluid density (1.225 kg/m3), and inlet fluid velocity (10, 14, 20, 24, 26, and 30 m/s). The simulations' output parameters include velocity and pressure measured at two points: section A-A (before the pipe bend) and section B-B (after pipe bend). The findings demonstrate that the velocity and pressure distribution is somewhat uneven at section B-B owing to the presence of the rotating vane. The most efficient rotation vane blade angle is 10° since it has the lowest velocity, static pressure, and pressure drop.

## 1. Introduction

The 90° pipe bend is often employed in pipeline systems to divert flow to specific places [1,2]. It is used in a variety of engineering applications, including the oil industry, transportation systems, water supply systems, air conditioning systems, and hydraulic systems [3–5]. As the fluids travel through the pipe bend, the turbulent flow of high-velocity fluids contacts the pipe bend's wall, and centrifugal force is created based on the bend curvature, resulting in the development of secondary flows [2]. Secondary flows may have led to pressure drop (or loss) [6,7]. An abrupt change in flow direction in a pipe bend causes corrosion and erosion [8–10]. These issues create pipe wall wear, leading in pipeline system failure, which has been claimed to be the major concern in the oil and gas sectors [11,12]. This failure resulted in a shutdown of production, economic losses, and increased pollution [10,12]. Wear is also a major issue in a variety of sectors, including mining [13],

* *Corresponding author.*
*E-mail address: mnormusa@utm.my*

https://doi.org/10.37934/arfmts.95.2.8498

transportation [14], lubrication [15-20] and manufacturing [21-23]. As a result, it is critical to find a solution to these issues.

Saha [3] numerically investigated the influence of guide vanes on fluid flow characteristics and discovered that secondary flow was nonexistent when guide vanes were inserted in pipe bends. Valsala [7] also used a guiding vane to prevent pressure loss at pipe bends. They used numerical analysis to investigate the impacts of vane number and shape on flow characteristics. Their research found that choosing the right vane number and fin design may significantly minimize turbulence and secondary flow, lowering pressure loss. Several investigations have also been conducted to directly evaluate the relationship between corrosion failures and particle properties and flow characteristics. Li [12] discovered that corrosion failures in pipes are affected by particle concentrations and flow characteristics (i.e., temperature and velocity) using numerical simulation studies. Singh [8] studied the relationship between erosion wear and velocity, particle size, and concentrations of sand water slurry flowing through a pipe bend numerically. The findings found that erosion increased dramatically with these conditions. To prevent corrosion and erosion issues in pipe bends, it is vital to pay attention to these factors, which include particle properties (size and concentration) and flow characteristics (secondary flow, temperature, and velocity).

The above-mentioned literature mostly conducted their investigations numerically because experimental research is expensive and time consuming [24]. Computational fluid dynamics (CFD) is a useful method for solving fluid flow problems by using Navier-Stokes equation and the suitable boundary conditions [8]. CFD is extensively used because it is user-friendly, can save energy, time, and money on experimentation, can accomplish accurate fluid flow prediction, and can provide results efficiently [25,26].

The current study attempts to control flow characteristics such as velocity and pressure drop in a 90° pipe bend by inserting a Cheng rotation vane (CRV) within the pipe. CRV was chosen because it is extensively utilized in various industries to handle pipe bend erosion issues by eliminating turbulence, reducing fluid velocity, and reducing pressure drop in pipe bends [27]. The flow characteristics in the 90° pipe bend are numerically investigated using computational fluid analysis (CFD). The effects of varied rotating vane blade angles on flow characteristics such as fluid velocity, pressure, and pressure drop within the pipe bend were investigated.

## 2. Governing Equations and Numerical Methodology

Fluid flow across a 90° pipe bend is deemed incompressible. The three-dimensional Reynolds Averaged Navier-Stokes (RANS) equations were solved using the commercial computational fluid dynamics (CFD) program ANSYS AIM. Navier-Stokes equations are made up of governing equations such as mass conversion, Eq. (1), and momentum conversion, Eq. (2).

$$\frac{\delta u_i}{\delta x_i} = 0 \tag{1}$$

$$\frac{\delta u_i}{\delta t} + u_j \frac{\delta u_i}{\delta x_j} = f_i - \left[\frac{1}{\rho}\frac{\delta p}{\delta x_i}\right] + \upsilon \frac{\delta^2 u_i}{\delta x_j \delta x_j} \tag{2}$$

where $f_i$ is the vector representing external force and $\upsilon$ is the kinematic viscosity.

The present study focuses on the impacts of various rotating vane blade angles on the velocity distribution, pressure distribution, and pressure drop characteristics in a pipe bend. The pipe bend geometry, illustrated in Figure 1, was created using SolidWorks software, and the geometry's details are provided in Table 1. The velocity distribution, pressure distribution, and pressure drop were determined at sections A-A and B-B along (P1-P10), where pipe section A-A is located 0.1m before the fluid enters the rotation vane at the vertical pipe and section B-B is located 0.1m after the fluid passes through the rotation vane at the horizontal pipe, as shown in Figure 1(a). In this investigation, two distinct rotation vane blade angles of 10° and 33° were adopted, as illustrated in Figure 1(b) and 1(c), respectively. Figure 2 shows the mesh distribution of the pipe created by ANSYS software. Because of its capacity to resolve an exact flow and outcomes, hexahedral mesh was utilized. The computational domain's grid generation consists of roughly 210591 and 209662 meshes for 10° and 33° rotation vane blade models, respectively.

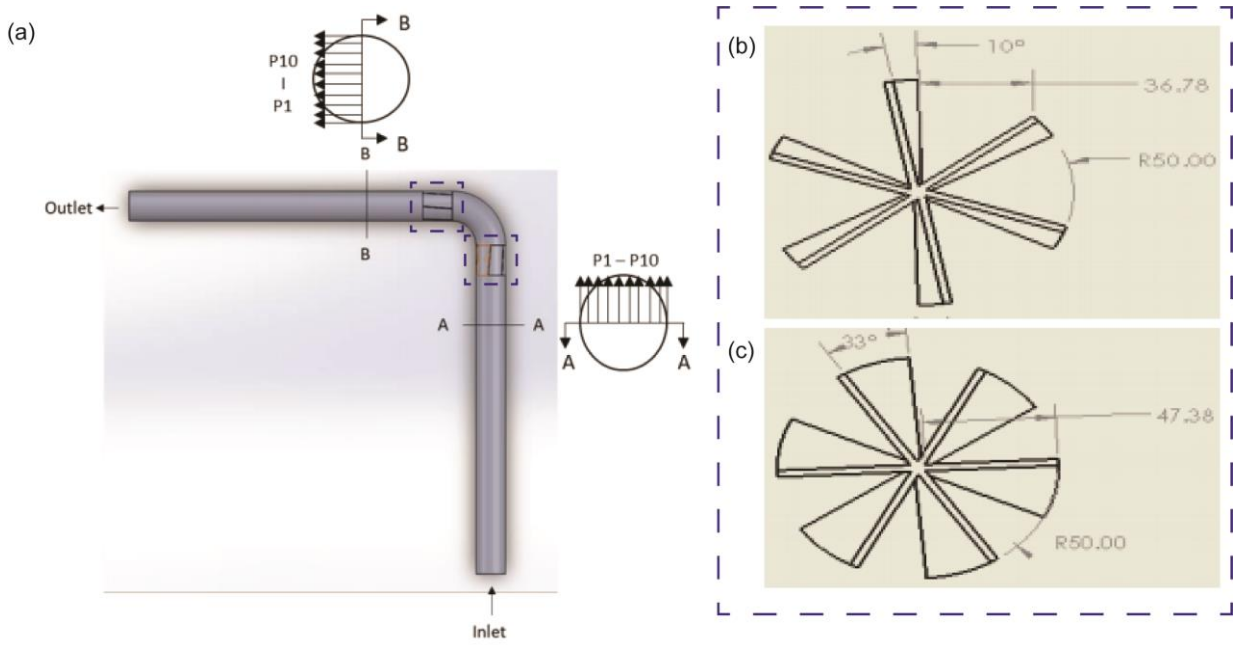


**Fig. 1.** Geometric models of (a) a pipe, (b) a rotation vane blade with a 10° angle, and (c) a rotation vane blade with a 33° angle

**Table 1**
Geometry description

| Diameter (m) | Vertical length (m) | Horizontal length (m) | Rotation vane blade angle (°) | Rotation vane blade material | Material density (kg/m$^3$) |
|---|---|---|---|---|---|
| 0.1 | 1 | 1 | 10, 33 | Steel | 8030 |

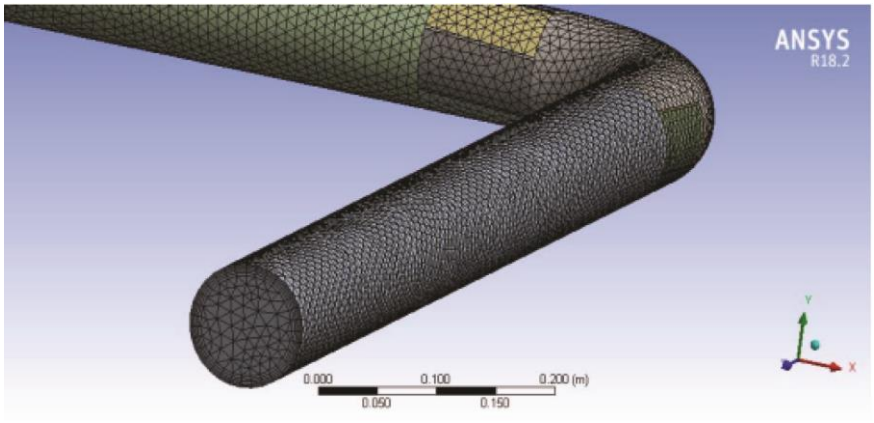


**Fig. 2.** Mesh scheme of pipe bend cross section

The current research focuses on multiphase flow, turbulent flow, and steady state. For addressing the governing equations, the realizable k-ε turbulence model was adopted. This model was chosen because it is known to offer accurate predictions, the best fit with experimental data, it is suited for solving intricate flows, and it works better for single-phase flows in pipe bends [3,28]. The governing equations for k-ε are given in [3]. The standard wall function was employed for near wall treatment because it allowed for the use of a reasonably coarse mesh in the pipe's near wall area. The SIMPLE algorithm and second order upwind techniques were used for pressure-velocity coupling. Air is used as the working fluid in this investigation. In order to increase the Reynolds number, the input velocity was changed in each numerical model. The following initial boundary conditions were considered in this study: (i) the temperature effect was negligible; (ii) the flow regime was assumed to be transient; (iii) no phase changes and no mass transfer between phases; (iv) the inlet was defined at the lower vertical pipe, whereas the outlet was defined at the end of the horizontal pipe; and (v) all the outer surfaces of the geometry declared as a wall. Table 2 shows the complete list of parameters utilized in this investigation.

**Table 2**
Simulation setup used in this study

| Parameters | Settings | |
|---|---|---|
| Turbulence model | Realizable k-ε | |
| Near wall | Standard wall functions | |
| Pressure-viscosity coupling | Simple | |
| Fluid | Air | |
| Air density | 1.225 kg/m$^3$ | |
| Air viscosity | 0.000017894 kg/m.s | |
| Operating pressure | Atmospheric | |
| Inlet velocity | V (m/s) | Re |
| | 10 | 68458.70 |
| | 14 | 95842.18 |
| | 20 | 136917.40 |
| | 24 | 164300.88 |
| | 26 | 177992.62 |
| | 30 | 205376.10 |

## 3. Validation of Numerical Model

To validate the accuracy of the simulation model, the current simulation results are validated with experimental data from [11]. The experiment in Asus's [11] was carried out utilizing a 90° pipe bend with a diameter of 0.054 m. The fluid characteristics employed in the previous investigation were similar with the current investigation.

## 4. Results and Discussion

The effects of varying angles of rotation vane blades on the velocity distribution, pressure distribution, and pressure drop characteristics in a pipe bend are numerically examined in this section. The simulation results were conducted at varied velocity inlet (V=10, 14, 20, 24, 26 and 30 m/s) at ten distinct places throughout the pipe cross-section with 0.01m spacing between two-points.

### *4.1 Velocity Distributions*

Figure 3 and 4 depict the velocity contour and velocity distributions of the pipe bend at different velocities with rotation vane blade angles of 10° and 33°. In general, these figures illustrate that the velocity distribution rises with increasing Reynolds number and illustrate the turbulent profile. The velocity distributions at section A-A were found to be identical for both rotation vane blade angles, as shown in Figure 3 and Figure 4(a) and (c). Because of the viscosity of the fluid that adheres to the pipe wall, the fluid viscosities at the pipe wall (P1 and P10) were equal to zero [24]. Figure 4 (a) and (c) show that the fluid velocity at section A-A rose from P2 to P4, then remained constant from P4 to P7 before decreasing from P7 to P9. These results reveal that the fluid velocity was at its greatest in the middle of the pipe cross-section.

Furthermore, the velocity contours vary after passing through the rotating vane blades. Fluid velocity was marginally higher in section B-B than in section A-A for both rotating vane blade angles. Figure 4(b) and (d) show that the fluid velocity of the pipe bends with rotation vane blade at 10° was smaller than that at 33°. The fluid velocity at section B-B for both rotation vane blade angles decreased from P2 to P6, then remained constant at P6 and P7 before rising again from P8 to P9. When compared to the velocity distributions at section A-A, which indicate more fluid velocity in the middle of the pipe section, the velocity distributions at section B-B indicate less fluid velocity in the middle of the pipe section. The existence of the rotating vane blade, which serves as a barrier for the fluid to pass along the pipe, causes this phenomenon [27].

Table 3 shows the maximum and minimum velocity at sections A-A and B-B of a pipe bend with rotating vane blades of 10° and 33° angles. According to Table 3, the maximum value of fluid velocity at section B-B was somewhat greater than that at section A-A due to the fluid flowing through the pipe bend. When compared to the velocity at section B-B, the highest velocity at section A-A was approximately identical to the inlet velocity. For each section, the lowest velocity at the pipe's wall is equal to zero. Furthermore, Table 3 reveals that the fluid velocity of a pipe bend with a rotation vane blade of 10° angle was lower than that of a pipe bend with a rotation vane blade of 33° angle. The velocity of a pipe bend with a 33° rotation vane blade (v=34.42 m/s) was 4% greater than that of a 10° rotation vane blade (v=33.10 m/s) at Re number 205376.10. Lower fluid velocity is preferred because it results in a lower pressure drop throughout the pipe section [11].

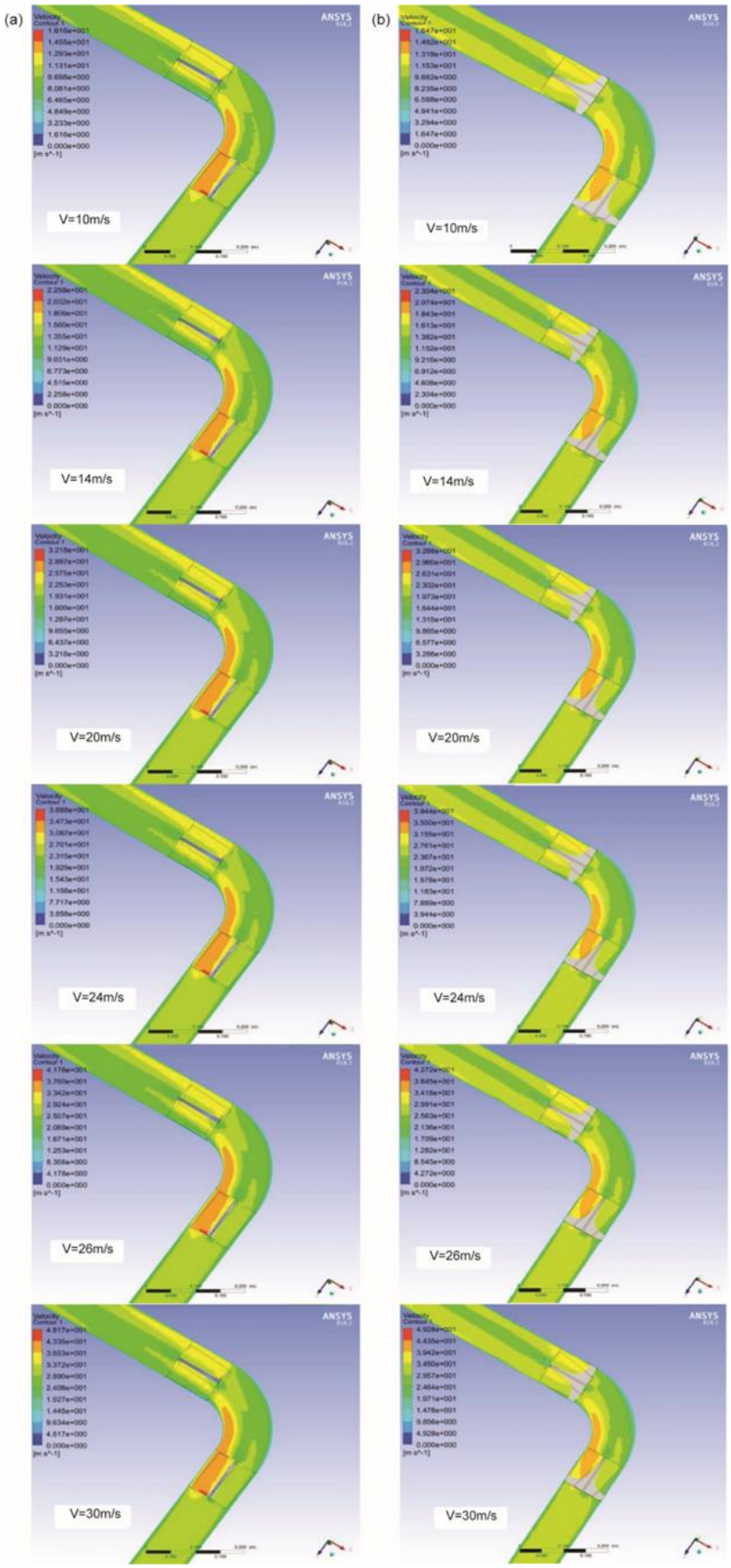


**Fig. 3.** Velocity contours of the pipe bend with rotating vane blade angles of (a) 10° and (b) 33° at various velocities

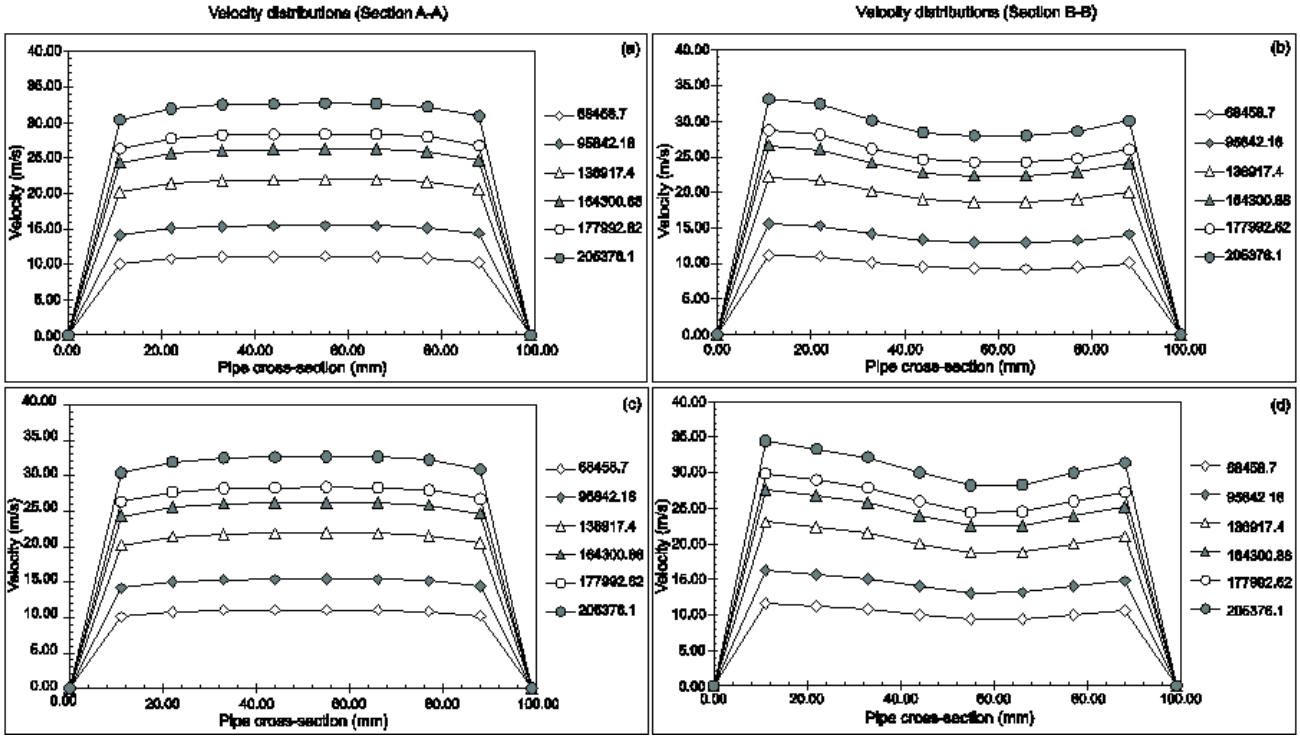


**Fig. 4.** Velocity distribution at sections A-A and B-B of the pipe bend with rotating vane blade angles of (a)-(b) 10° and (c)-(d) 33° at various velocities

**Table 3**
Maximum and minimum velocity at section A-A and section B-B of pipe bend with rotation vane blade of 10° and 33° angles the density of the specimen

| Velocity inlet, V (m/s) | Reynolds number, Re | Velocity at section A-A (10°) and (33°) | | Velocity at section B-B (10°) | | Velocity at section B-B (33°) | |
|---|---|---|---|---|---|---|---|
| | | Maximum | Minimum | Maximum | Minimum | Maximum | Minimum |
| 10 | 68458.70 | 11.09 | 0.00 | 11.15 | 0.00 | 11.64 | 0.00 |
| 14 | 95842.18 | 15.43 | 0.00 | 15.56 | 0.00 | 16.22 | 0.00 |
| 20 | 136917.40 | 21.91 | 0.00 | 22.15 | 0.00 | 23.06 | 0.00 |
| 24 | 164300.88 | 26.22 | 0.00 | 26.54 | 0.00 | 27.62 | 0.00 |
| 26 | 177992.62 | 28.37 | 0.00 | 28.73 | 0.00 | 29.89 | 0.00 |
| 30 | 205376.10 | 32.67 | 0.00 | 33.10 | 0.00 | 34.42 | 0.00 |

### *4.2 Pressure Distributions*

Figure 5 and 6 display the pressure contour and pressure distributions of the pipe bend with rotation vane blade angles of 10° and 33° at various velocities. Figure 5 and 6 illustrate that the pressure distributions throughout the pipe cross-section are affected by the Reynolds number. As the Reynolds number rises, so do the pressure distributions. Figure 6(a) and 6(b) indicate that the pressure distributions at section A-A vary very little over the pipe cross-section (from P2 to P9) for both rotating vane blade angles, see Figure 6(a) and (c).

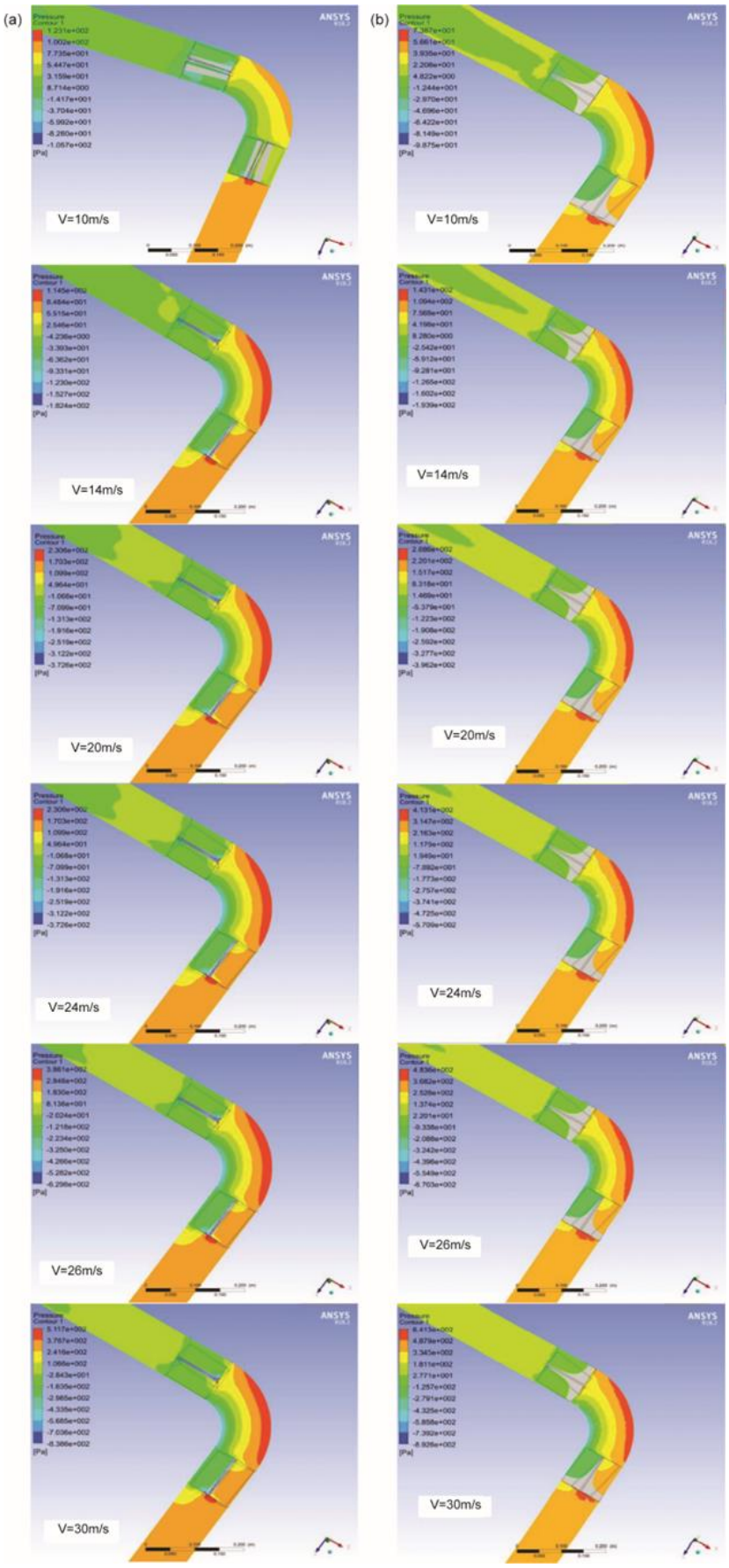


**Fig. 5.** Pressure contours of the pipe bend with rotation vane blade angles of (a) 10° and (b) 33° at various velocities

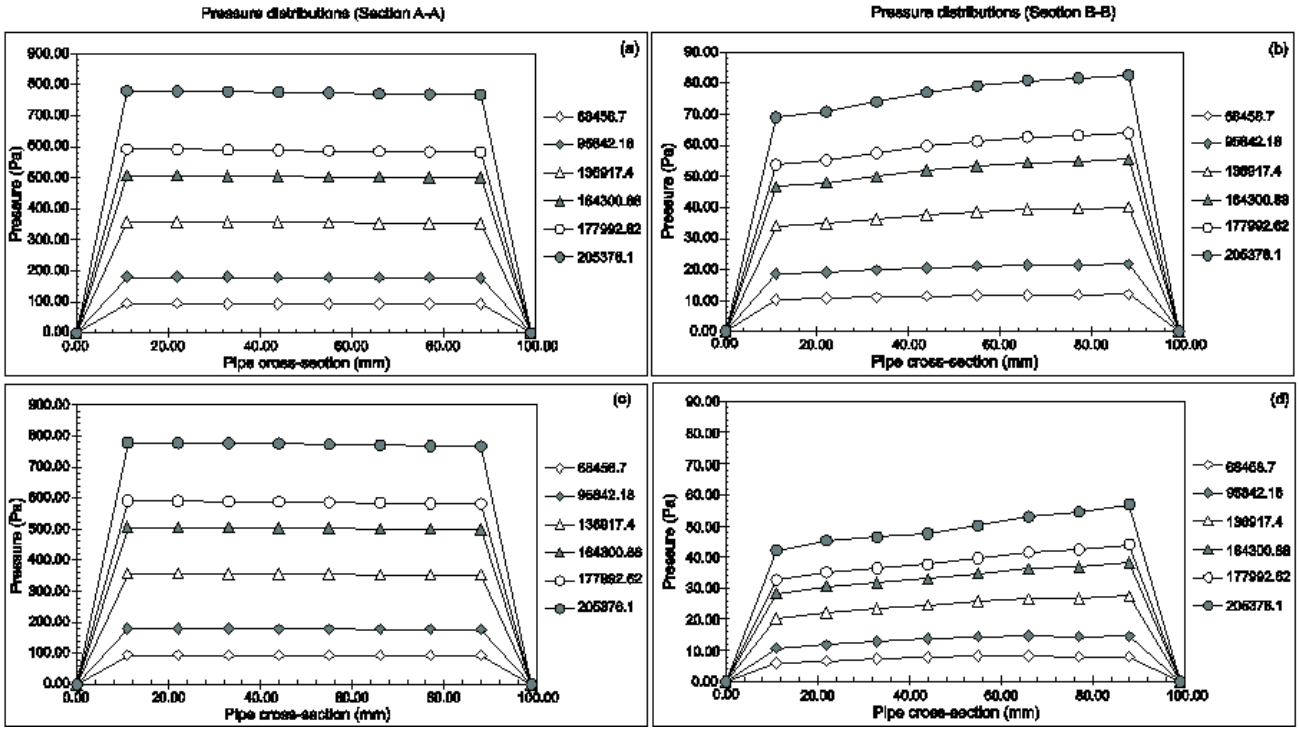


**Fig. 6.** Pressure distribution at sections A-A and B-B of the pipe bend with rotating vane blade angles of (a)-(b) 10° and (c)-(d) 33° at various velocities

Figure 6(b) and (d) show the pressure distributions at section B-B for both rotation vane blade angles. It is evident that the pressure inside the pipe became lower after the fluid passing through the rotation vane blade. The pressure distributions at section B-B for both rotating vane blade angles exhibit a similar pattern, indicating an increase in pressure from P2 to P9. However, the pressure value varies slightly owing to changes in rotating vane angle. The pressure across the pipe cross-section of a rotation vane blade angle of 10° was greater than that of a rotation vane blade angle of 33°. Because of momentum exchanges and normalized pressure from the uniform value of static pressure before the fluid flows through the rotating vane blade to the curvature of the pipe bend, the pressure increment across the pipe cross-section rises from the bottom to the upper part section [6]. The pressure drops slightly from the lower to upper part of section B-B due to the centrifugal force caused by the circular motion of fluid particles caused by the curvature of the pipe bend [29].

Table 4 shows the maximum and minimum pressures at sections A-A and B-B of a pipe bend with rotating vane blades at 10° and 33° angles. This table clearly illustrates that the maximum pressure in section B-B was lower than in section A-A. This happened as a result of the geometry model's curvature. The greatest pressure was found to be at the top part of the pipe cross-section (P9) at section B-B of the pipe bend, while the lowest pressure was found to be at the lower part of the pipe cross-section (P2). As shown in Table 4, the pressure of a pipe bend with a rotation vane blade of 10° angle was greater than that of a pipe bend with a rotation vane blade of 33° angle. The pressure of a pipe bend with a 10° rotation vane blade (P=82.59 Pa) was 31% greater than that of a 33° rotation vane blade (P=56.92 Pa) at Re number 205376.10. The greater the pressure, the greater the fluid velocity. According to the findings of the velocity distributions in the previous section, the fluid velocity of a pipe bend with a rotating vane blade of 10° angle was lower. The installation of a rotating vane blade with a 10° angle has reduced fluid velocity, resulting in a lower pressure drop when the fluid passes through the pipe bend.

**Table 4**
Maximum and minimum pressure at section A-A and section B-B of pipe bend with rotating vane blade of 10° and 33° angles

| Velocity inlet, V (m/s) | Reynolds number, Re | Pressure at section A-A (10°) and (33°) | | Pressure at section B-B (10°) | | Pressure at section B-B (33°) | |
|---|---|---|---|---|---|---|---|
| | | Maximum | Minimum | Maximum | Minimum | Maximum | Minimum |
| 10 | 68458.70 | 94.58 | 0.00 | 11.93 | 0.00 | 8.32 | 0.00 |
| 14 | 95842.18 | 179.82 | 0.00 | 21.67 | 0.00 | 14.56 | 0.00 |
| 20 | 136917.40 | 357.00 | 0.00 | 40.08 | 0.00 | 27.47 | 0.00 |
| 24 | 164300.88 | 506.73 | 0.00 | 55.46 | 0.00 | 38.09 | 0.00 |
| 26 | 177992.62 | 591.05 | 0.00 | 63.96 | 0.00 | 43.98 | 0.00 |
| 30 | 205376.10 | 778.65 | 0.00 | 82.59 | 0.00 | 56.92 | 0.00 |

### *4.3 Pressure Drop*

Figure 7 depicts the pressure drop between sections A-A and B-B of the pipe bend with rotating vane blade angles of 10° and 33° at different velocities. The graph indicates that the pressure loss rises dramatically with Reynolds number for both rotating vane blade angles. The pressure changed from section A-A to section B-B as a result of centrifugal forces, friction on the pipe bend wall, and the angle of rotation of the vane blade [5,30]. The largest pressure drop happened at the lower end of the pipe cross-section (P2), while the least pressure drop happened at the higher end of the pipe cross-section (P9). However, the difference in pressure drop between these two points is relatively marginal for each Reynolds number. Table 5 contains the data for the maximum pressure drop for both rotating vane blade angles. This table illustrates that as the Reynolds number increased, the maximum pressure drop raised dramatically. This table's data also illustrate that the angle of rotation of the vane blade impacts the pressure drop. In comparison, the pressure drop for a rotation vane blade with a 10° angle was less than that of a rotation vane blade with a 33° angle. The pressure drop of a pipe bend with a 10° rotation vane blade (P=709.6 Pa) was 3.8% lower than that of a 33° rotation vane blade (P=736.54 Pa) at Re number 205376.10. The minimum pressure drop is critical since it is the primary criterion that may impact pipe system efficiency. As a result, a rotating vane blade with a 10° angle is the ideal angle since it delivers the least amount of fluid velocity and pressure decrease.

**Table 5**
Maximum and minimum pressure drop between Sections A-A and section B-B of pipe bend with rotating vane blade of 10° and 33° angles

| Velocity inlet, V (m/s) | Reynolds number, Re | Pressure drop between sections A-A and B-B (10°) | | Pressure drop between sections A-A and B-B (33°) | |
|---|---|---|---|---|---|
| | | Maximum | Minimum | Maximum | Minimum |
| 10 | 68458.70 | 84.19 | 0.00 | 88.66 | 0.00 |
| 14 | 95842.18 | 161.15 | 0.00 | 169.07 | 0.00 |
| 20 | 136917.40 | 322.98 | 0.00 | 336.60 | 0.00 |
| 24 | 164300.88 | 460.00 | 0.00 | 478.50 | 0.00 |
| 26 | 177992.62 | 537.30 | 0.00 | 558.48 | 0.00 |
| 30 | 205376.10 | 709.60 | 0.00 | 736.54 | 0.00 |

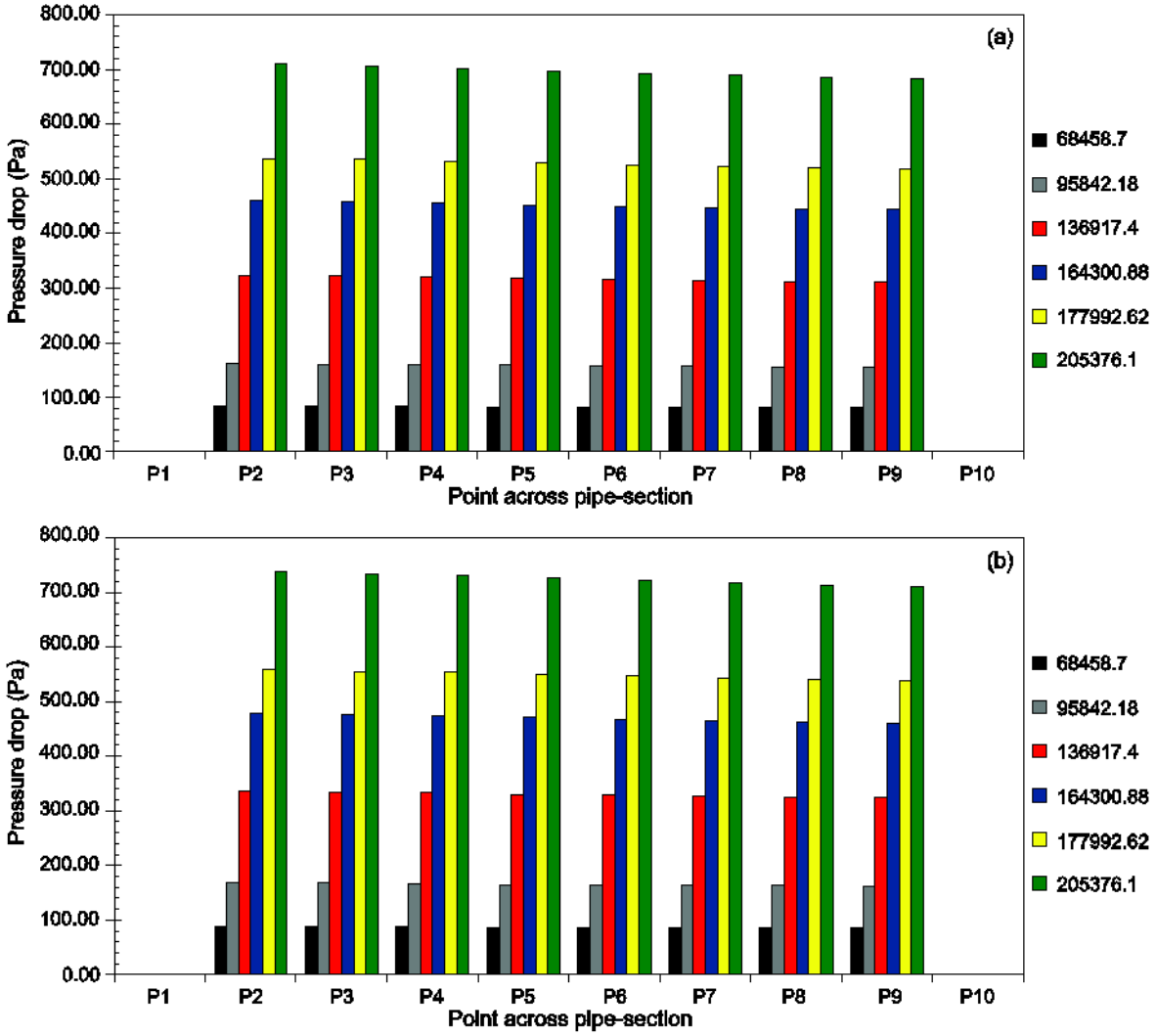


**Fig. 7.** Pressure drop between sections A-A and B-B of the pipe bend with rotating vane blade of angles (a) 10° and (b) 33°

### *4.4 Validation*

Table 6 compares the maximum and minimum velocity findings of the simulation analysis with the experiment findings obtained by Asus [11], which were obtained by measuring the velocity distribution at section B-B of a pipe bend with rotating vane blades of 10° and 33° angles. The maximum velocity value for the 33° rotation vane was larger for both Re numbers than for the 10° rotation vane, indicating extremely strong agreement between simulation and experimental data. Table 6 shows that the percentage discrepancy between the simulation and experiment findings is roughly 23% for both rotating vane blade angles. Despite a velocity differential of 23%, simulation findings indicate a relatively good agreement with experimental data. The inaccuracy was caused by the differing pipe diameter sizes employed in both tests. The velocity is greater in the experiment because the pipe diameter was two times smaller than in the current investigation.

**Table 6**
Velocity distribution validation of experimental data of Asus [11] with present simulation

| Velocity inlet, V (m/s) | Reynolds number, Re | Simulation | | | | Experiment | | | | Percentage different from the previous study | |
|---|---|---|---|---|---|---|---|---|---|---|---|
| | | Velocity at section B-B (10°) | | Velocity at section B-B (33°) | | Velocity at section B-B (10°) | | Velocity at section B-B (33°) | | | |
| | | Max | Min | Max | Min | Max | Min | Max | Min | (10°) | (33°) |
| 26 | 177992.62 | 28.73 | 0.00 | 29.89 | 0.00 | 37.38 | 0.00 | 38.87 | 0.00 | 23.15% | 23.11% |
| 30 | 205376.10 | 33.10 | 0.00 | 34.42 | 0.00 | 43.23 | 0.00 | 44.70 | 0.00 | 23.42% | 23.01% |

Table 7 shows a comparison of the pressure distribution at section B-B of a pipe bend with rotating vane blades of 10° and 33° angles between simulated analysis and experimental data. According to Asus [11], the maximum pressure achieved was negative because the pressure at section A-A was larger than that at section B-B. According to Table 7, there is a large percentage discrepancy between the simulation and experimental data, ranging from 92% to 95%. This circumstance happened as a result of the pressure boundary conditions chosen at the end of the pipe model in simulation. For the fluid to flow out of the pipe, the outflow boundary conditions were specified. The gauge pressure in the prior experiment design is unknown, which might limit the boundary condition setting. Because of the constraint, the outflow boundary conditions were used instead of the pressure outlet boundary condition, which might result in differing pressure values along with the pipe model.

**Table 7**
Pressure distribution validation of experimental data of Asus [11] with present simulation

| Velocity inlet, V (m/s) | Reynolds number, Re | Simulation | | | | Experiment | | | | Percentage different from the previous study | |
|---|---|---|---|---|---|---|---|---|---|---|---|
| | | Pressure at section B-B (10°) | | Pressure at section B-B (33°) | | Pressure at section B-B (10°) | | Pressure at section B-B (33°) | | | |
| | | Max | Min | Max | Min | Max | Min | Max | Min | (10°) | (33°) |
| 26 | 177992.62 | 63.96 | 0.00 | 43.98 | 0.00 | -842.14 | 0.00 | -910.69 | 0.00 | 92.41% | 95.17% |
| 30 | 205376.10 | 82.59 | 0.00 | 56.92 | 0.00 | -1126.12 | 0.00 | -1204.46 | 0.00 | 92.67% | 95.27% |

Table 8 compares the pressure drop between the experimental and simulation findings of the current investigation. Table 8 shows that the pressure drop trend for simulation findings matches the experimental data, indicating that the pressure drop with 33° rotation vane is greater than that with 10° rotation vane. The percentage difference in pressure drop between simulation and experimental data was less than 10%.

**Table 8**
Pressure drop validation of experimental data of Asus [11] with present simulation

| Velocity inlet, V (m/s) | Reynolds number, Re | Simulation | | | | Experiment | | | | Percentage different from the previous study | |
|---|---|---|---|---|---|---|---|---|---|---|---|
| | | Pressure at section B-B (10°) | | Pressure at section B-B (33°) | | Pressure at section B-B (10°) | | Pressure at section B-B (33°) | | | |
| | | Max | Min | Max | Min | Max | Min | Max | Min | (10°) | (33°) |
| 26 | 177992.62 | 537.30 | 0.00 | 558.48 | 0.00 | 509.20 | 0.00 | 577.75 | 0.00 | 5.52% | 3.34% |
| 30 | 205376.10 | 709.60 | 0.00 | 736.54 | 0.00 | 705.05 | 0.00 | 802.97 | 0.00 | 0.65% | 8.27% |

## 4. Conclusions

The air flow through a 90° pipe bend was computationally examined using computational fluid analysis (CFD) simulations at various inlet velocities ranging from 10 m/s to 30 m/s and Reynolds numbers ranging from 68458.70 to 205376.10. The velocity distribution, pressure distribution, and pressure drop are presented and analysed for rotating vane angles of 10° and 33°. The current investigation leads to the following conclusions

i. For both pipe bends with rotating vane blade angles of 10° and 33°, the velocity, pressure, and pressure loss increased as the Reynolds number increased. Before the fluid passed through the rotating vane blade, a uniform velocity profile was developed. Then, in the middle of the pipe bend, it becomes uneven and reaches maximum velocity in the upper section of the pipe. This occurrence happened as a result of the curvature and rotation vane blade, which serve as a barrier to fluid flow.
ii. The pressure distribution along the pipe model is inversely proportional to the velocity profile. These findings are consistent with the momentum equation theory, which includes potential energy, kinetic energy, and pressure. As the velocity represented by kinetic energy rises, the pressure must decrease in proportion to maintain all points along a streamline constant. In addition, when the fluid flows through the pipe bend, the pressure tends to decrease, causing the velocity to rise. As a result, pressure drops occurred at several pipe bends throughout the pipeline system.
iii. It has been discovered that by inserting a vane blade in the pipes system, the separation flow may be removed. The fluids that flow through the 10° rotation vane blade angle have lower velocity, pressure, and pressure drop than the fluids that flow through the 33° rotation vane blade angle. In the current investigation, the optimal rotation vane angle is 10° because smaller pressure drop produced implies greater flow system efficiency.
iv. The validation of the current simulation with the experiments given in Reference [11] reveals a similar pattern. The findings reveal that the percentage difference in velocity and pressure drop was smaller owing to differences in pipe diameter, whereas the percentage difference in pressure was greater owing to the pressure boundary conditions settings.

## Acknowledgement

The authors would like to express their thanks to the Ministry of Higher Education of Malaysia for the FRGS Grant (FRGS/1/2019/TK03/UTM/02/18), Universiti Teknologi Malaysia (UTM) for the Research University Grant (21H50), TDR Grant (05G23) and FRGS Grant (5F074, 5F173). The authors also like to thank Malaysia – Japan International Institute of Technology (MJIIT) and Takasago Thermal Engineering for funding this work under the grant R.K130000.7343.4B631.

## References

[1] Ayala, Manuel, and John M. Cimbala. "Numerical approach for prediction of turbulent flow resistance coefficient of 90° pipe bends." *Proceedings of the Institution of Mechanical Engineers, Part E: Journal of Process Mechanical Engineering* 235, no. 2 (2021): 351-360. https://doi.org/10.1177/0954408920964008

[2] Sigalotti, Leonardo Di G., Carlos E. Alvarado-Rodríguez, Jaime Klapp, and José M. Cela. "Smoothed Particle Hydrodynamics Simulations of Water Flow in a 90° Pipe Bend." *Water* 13, no. 8 (2021): 1081. https://doi.org/10.3390/w13081081

[3] Saha, Sumit Kumar, and Nityananda Nandi. "Change in flow separation and velocity distribution due to effect of guide vane installed in a 90 pipe bend." *Mechanics and Mechanical Engineering* 21, no. 2 (2017): 353-361.

[4] Zhang, Chi, Angui Li, Jigang Che, Yue Li, Qi Liu, and Yuhang Zhao. "A low-resistance elbow with a bionic sawtooth

guide vane in ventilation and air conditioning systems." In *Building Simulation*, vol. 15, no. 1, pp. 117-128. Tsinghua University Press, 2022. https://doi.org/10.1007/s12273-021-0782-y

[5] Korkmaz, Y. Selim, A. Kibar, and K. Suleyman Yigit. "Experimental and Numerical Investigation of Flow in Hydraulic Elbows." *Journal of Applied Fluid Mechanics* 14, no. 4 (2021): 1137-1146. https://doi.org/10.47176/jafm.14.04.32243

[6] Dutta, Prasun, Sumit Kumar Saha, Nityananda Nandi, and Nairit Pal. "Numerical study on flow separation in 90° pipe bend under high Reynolds number by k-ε modelling." *Engineering Science and Technology, an International Journal* 19, no. 2 (2016): 904-910. https://doi.org/10.1016/j.jestch.2015.12.005

[7] Valsala, Reji Reghunathan, S. W. Son, Abhilash Suryan, and Heuy Dong Kim. "Study on reduction in pressure losses in pipe bends using guide vanes." *Journal of Visualization* 22, no. 4 (2019): 795-807. https://doi.org/10.1007/s12650-019-00561-w

[8] Singh, V., S. Kumar, and S. K. Mohapatra. "Modeling of erosion wear of sand water slurry flow through pipe bend using CFD." *Journal of Applied Fluid Mechanics (JAFM)* 12, no. 3 (2019): 679-687. https://doi.org/10.29252/jafm.12.03.29199

[9] Zeng, Li, Geng Chen, and Hanxin Chen. "Comparative study on flow-accelerated corrosion and erosion–corrosion at a 90 carbon steel bend." *Materials* 13, no. 7 (2020): 1780. https://doi.org/10.3390/ma13071780

[10] Jia, Wenlong, Yuanrui Zhang, Changjun Li, Peng Luo, Xiaoqin Song, Yuzhu Wang, and Xinyi Hu. "Experimental and numerical simulation of erosion-corrosion of 90° steel elbow in shale gas pipeline." *Journal of Natural Gas Science and Engineering* 89 (2021): 103871. https://doi.org/10.1016/j.jngse.2021.103871

[11] Asus, K., 2014. Air Flow Analysis and Effect of Angle On Rotation Vane Blade Through 90 Degree Pipe Bend. Universiti Teknologi Malaysia, Johor Bahru: Tesis Ijazah Sarjana Muda.

[12] Li, Ping, Yang Zhao, Bin Liu, Guanxin Zeng, Tao Zhang, Dake Xu, Hong Gu, Tingyue Gu, and Fuhui Wang. "Experimental testing and numerical simulation to analyze the corrosion failures of single well pipelines in Tahe oilfield." *Engineering Failure Analysis* 80 (2017): 112-122. https://doi.org/10.1016/j.engfailanal.2017.06.014

[13] Calderon-Hernandez, Jose Wilmar, Amilton Sinatora, Hercilio G. de Melo, Arthur P. Chaves, Eliana S. Mano, Laurindo S. Leal Filho, Jose L. Paiva, Andre S. Braga, and Thiago C. Souza Pinto. "Hydraulic convey of iron ore slurry: Pipeline wear and ore particle degradation in function of pumping time." *Wear* 450 (2020): 203272. https://doi.org/10.1016/j.wear.2020.203272

[14] Peng, Guangjie, Xin Huang, Ling Zhou, Guoxin Zhou, and Hong Zhou. "Solid-liquid two-phase flow and wear analysis in a large-scale centrifugal slurry pump." *Engineering Failure Analysis* 114 (2020): 104602. https://doi.org/10.1016/j.engfailanal.2020.104602

[15] Hassan, Mohammed, Farid Nasir Ani, and S. Syahrullail. "Tribological performance of refined, bleached and deodorised palm olein blends bio-lubricants." Journal of Oil Palm Research 28.4 (2016): 510-519. https://doi.org/10.1016/j.wear.2020.203272

[16] Syahrullail, S., Kamitani, S., & Nakanishi, K. "Experimental evaluation of refined, bleached, and deodorized palm olein and palm stearin in cold extrusion of aluminum A1050." *Tribology Transactions* 55(2) (2012): 199-209. https://doi.org/10.1080/10402004.2011.648826

[17] Golshokouh, Iman, Mohamadali Golshokouh, Farid Nasir Ani, Ehsan Kianpour, and S. Syahrullail. "Investigation of physical properties for jatropha oil in different temperature as lubricant oil." *Life Science Journal* 10, no. 8 (2013): 110-119.

[18] Golshokouh, I., Syahrullail, S., Ani, F. N., & Masjuki, H. H. "Investigation of palm fatty acid distillate oil as an alternative to petrochemical based lubricant." *Journal of Oil Palm Research* 26(1), (2014): 25-36.

[19] Wannik, W. B., Ayob, A. F., Syahrullail, S., Masjuki, H. H., & Ahmad, M. F. "The effect of boron friction modifier on the performance of brake pads." *International Journal of Mechanical and Materials Engineering* 7(1) (2012): 31-35.

[20] Azman, N. F., Samion, S., & Sot, M. N. H. M. "Investigation of tribological properties of CuO/palm oil nanolubricant using pin-on-disc tribotester." *Green materials* 6(1) (2018): 30-37. https://doi.org/10.1680/jgrma.17.00026

[21] Syahrullail, S., Nakanishi, K., & Kanitani, S. (2005). "Investigation of the effects of frictional constraint with application of palm olein oil lubricant and paraffin mineral oil lubricant on plastic deformation by plane strain extrusion." *Japanese Journal of Tribology*, 50, no.6 (2005): 727-738.

[22] Golshokouh, I., et al. "Investigation of palm fatty acid distillate as an alternative lubricant of petrochemical based lubricants, tested at various speeds." International Review of Mechanical Engineering 7.1 (2013): 72-80.

[23] Yahaya, Aiman, Syahrullail Samion, and Mohamad Nor Musa. "Determination of friction coefficient in the lubricated ring upsetting with palm kernel oil for cold forging of aluminum alloys." *Jurnal Tribologi* 25 (2020): 16-28.

[24] Qing, Nelvin Kaw Chee, Nor Afzanizam Samiran, and Razlin Abd Rashid. "CFD Simulation analysis of Sub-Component in Municipal Solid Waste Gasification using Plasma Downdraft Technique." *Journal of Advanced Research in Numerical Heat Transfer* 8, no. 1 (2022): 36-43.

[25] Elfaghi, Abdulhafid MA, Alhadi A. Abosbaia, Munir FA Alkbir, and Abdoulhdi AB Omran. "CFD Simulation of Forced Convection Heat Transfer Enhancement in Pipe Using Al2O3/Water Nanofluid." *Journal of Advanced Research in Numerical Heat Transfer* 8, no. 1 (2022): 44-49.
[26] Rasep, Zuraidah, Muhammad Noor Afiq Witri Muhammad Yazid, and Syahrullail Samion. "A study of cavitation effect in a journal bearing using CFD: A case study of engine oil, palm oil and water." *Jurnal Tribologi* 28 (2021): 48-62.
[27] Cheng Fluid System. Inc. "Flow Conditioning Technology: CRV and LAD" [Online]. Available: http://www.chengfluid.com/flow_problems/elbow_erosion.
[28] Xu, Lei, Dongtao Ji, Wei Shi, Bo Xu, Weigang Lu, and Linguang Lu. "Influence of inlet angle of guide vane on hydraulic performance of an axial flow pump based on CFD." *Shock and Vibration* 2020 (2020). https://doi.org/10.1155/2020/8880789
[29] Galvis, Nelson Enrique Barros. *Geomechanics, Fluid Dynamics and Well Testing, Applied to Naturally Fractured Carbonate Reservoirs: Extreme Naturally Fractured Reservoirs*. Springer, 2018. https://doi.org/10.3997/2214-4609.201800035
[30] Mazumder, Quamrul H. "CFD analysis of the effect of elbow radius on pressure drop in multiphase flow." *Modelling and Simulation in Engineering* 2012 (2012). https://doi.org/10.1155/2012/125405